Supporting Information

A Dual-Additive Strategy Constructing Robust Li_3N-Rich SEI and Proton Scavenging for High-Rate Lithium Metal Batteries

Dongxiang Li‡[a,b,c], Suyan Niu‡[b], Zhigang Zhang[a,c], Chen Yang[a,c], Boyun Wang[a,c], Zilong Liu[b], Na Ju[b], You Fu[b], Lei Shi[a,c], Guang-Wen Xu*[a,c], Hong-bin Sun*[a,b]*

Dongxiang Li, Zhigang Zhang, Chen Yang, Boyun Wang, Prof. Lei Shi, Prof. Guang-Wen Xu, Prof. Hong-bin Sun

a Key Laboratory on Resources Chemicals and Materials of Ministry of Education, Shenyang University of Chemical Technology, Shenyang 110142, People's Republic of China.

E-mail: sunhb@mail.neu.edu.cn, gwxu@syuct.edu.cn, sunhb@mail.neu.edu.cn

Dongxiang Li, Suyan Niu, Zilong Liu, Na Ju, You Fu, Prof. Hong-bin Sun

b Department of Chemistry, Northeastern University, Shenyang 110819, People's Republic of China.

E-mail: sunhb@mail.neu.edu.cn

Dongxiang Li, Zhigang Zhang, Chen Yang, Boyun Wang, Prof. Lei Shi, Prof. Guang-Wen Xu

c Institute of Industrial Chemistry and Energy Technology, Shenyang University of Chemical Technology, Shenyang 110142, People's Republic of China.

E-mail: shilei@syuct.edu.cn, gwxu@syuct.edu.cn

‡These authors contributed equally to this work.

1.1 Preparation of electrolyte and electrode

The benchmark commercial electrolyte (BE) used for battery-grade applications consists of 1 M $LiPF_6$ dissolved in EC/DEC (1:1, v/v) with 2 vol.% VC, purchased from Shanghai SongJing New-Energy Technology Limited. The CTZ electrolyte was prepared by dissolving dried 3-cyano-1,2,4-triazole (CTZ) into the BE electrolyte at a concentration of 0.05 wt.%. Subsequently, the CTZ+TMSIM electrolyte was obtained by further adding 1-(trimethylsilyl) imidazole (TMSIM) to the CTZ electrolyte, with a TMSIM-to-CTZ molar ratio of 1:1. All electrolyte preparation and cell assembly procedures were conducted in an argon-filled glove box with high-purity argon atmosphere.

$LiFePO_4$ (LFP) powder and N-methyl-2-pyrrolidone (NMP) were obtained from Aladdin, while acetylene black (ACET) and polyvinylidene fluoride (PVDF) were sourced from Guangdong Canrd New Energy Technology Co., Ltd. The cathode slurry was prepared with a weight ratio of LFP:ACET:PVDF = 8:1:1. First, LFP and ACET were thoroughly mixed and ground. PVDF was dissolved in NMP at a 1:9 ratio (PVDF:NMP) under continuous stirring until a clear solution formed. The LFP-ACET mixture was then combined with the PVDF-NMP solution and stirred until homogeneous. The slurry was coated onto cleaned aluminum foil (thickness 16 μm, 99.9% purity) with an active material loading of 5 mg cm^{-2}, dried, and punched into circular electrodes of 14 mm diameter. High-loading LFP (active mass loading = 11.25 mg cm^{-2}) and $LiNi_{0.8}Co_{0.1}Mn_{0.1}O_2$ (NCM811, active mass loading = 8.7 mg cm^{-2}), as well as 50 μm-thick lithium foil, were purchased from Guangdong Canrd New Energy Technology Co., Ltd. The copper foil current collector (Cu, 9 μm thick, 99.9% purity) was cut into 14 mm diameter disks and cleaned multiple times with hydrochloric acid followed by deionized water. Lithium metal foil (99.9% purity).

1.2 Electrochemical Testing

Electrochemical testing was conducted using coin-type batteries (CR2025) with Celgard PE as the separator and 30 μL of electrolyte. For Li||LFP batteries, cycling tests were performed at 0.5 C (1C = 170 mA g^{-1}) within the voltage range of 2.5 to 3.8 V. The battery's rate performance was evaluated at 0.1 C, 0.2 C, 0.3 C, 0.5 C, 1 C, 2 C, 3 C, 5 C, and 10 C. For the Li||NCM811 battery (1C = 200 mA g^{-1}), the voltage test range was 3-4.3 V.

The coulombic efficiency (CE) of lithium plating/stripping in different electrolytes was evaluated for Li||Cu batteries using the Aurbach method and the standard method.

Aurbach method: Initially, a pre-deposited lithium plating capacity (QT) equal to 2 or 3 times the fixed capacity was applied at a current density of 0.5 mA cm^{-2}, followed by n cycles of plating/stripping at a fixed capacity (QC = 1 mAh cm^{-2}). The retained capacity (QR) was measured during the final stripping step at 0.5 mA cm^{-2}. The CE was calculated as follows:

$$CE = \frac{nQ_C + Q_R}{nQ_C + Q_T}$$

Standard method: Lithium plating was conducted at a current density of 1 mA cm^{-2} with a fixed capacity of 1 mAh cm^{-2}, followed by stripping at the same current density to a cutoff voltage of 1 V to determine the coulombic efficiency for each cycle. Subsequent cycles were then performed under identical conditions.

The Li^+ transference number (t_{Li^+}) was determined via the Bruce-Vincent method using Li||Li symmetric cells. Amperometric current-time (i-t) tests applied a constant DC bias of 5 mV to measure the initial current (I_i) and steady-state current (I_s). Electrochemical impedance spectroscopy (EIS) was performed before and after the i-t test to obtain the initial (R_i) and steady-state (R_s) interfacial resistances over a frequency range of 100 kHz to 0.01 Hz with an AC amplitude of 10 mV. The t_{Li^+} was calculated as follows:

$$t_{Li+} = \frac{I_s \cdot (\Delta V - I_i \cdot R_i)}{I_i \cdot (\Delta V - I_s \cdot R_s)}$$

Cyclic voltammetry (CV) and electrochemical impedance spectroscopy (EIS) were conducted using a CHI760e electrochemical workstation. CV tests for Li||LFP cells were performed within a voltage window of 2.0-4.5 V at a scan rate of 0.1 mV s^{-1}. For Li||Cu half-

cells, CV measurements were carried out over a voltage range of -0.2 to 1.0 V at a scan rate of 0.5 mV s^{-1}. EIS was recorded across a frequency range from 100 kHz to 0.01 Hz.

1.3 Materials Characterization

UV – visible spectroscopy (UV2550) was employed to analyze the spectral shifts of the two additives. For the measurements, CTZ was dissolved in acetonitrile at a fixed concentration of 0.1 wt.%. Additionally, ^{1}H NMR analysis was performed using a Bruker AVANCE III 500 MHz superconducting spectrometer. CTZ and TMSIM were dissolved in DMSO-d6 at a concentration of 40 mg mL^{-1} and mixed at specific volume ratios (4:1 and 3:2, v/v) prior to measurement. The morphology of lithium metal was examined by scanning electron microscopy (SEM, JSM-IT800), energy-dispersive X-ray spectroscopy (EDS, Ultimax65), and atomic force microscopy (AFM, DIMENSION ICON). X-ray photoelectron spectroscopy (XPS) data were collected with a high-sensitivity Axis Supra+ spectrometer. Prior to characterization, electrode disks were rinsed three times with dimethyl carbonate (DMC) and dried in a glovebox. To analyze the cathode electrolyte interphase (CEI) formed after cycling, LFP material was gently scraped off the Al foil, ultrasonically dispersed in DMC, and drop-cast onto a copper grid for transmission electron microscopy (TEM) analysis (JEM-F200). After disassembling the cycled CTZ+TMSIM cells, the consumption and transformation of CTZ molecules during the cycle were characterized and verified using gas chromatography-mass spectrometry (GC-MS, Agilent7890A-5975C). Samples were prepared by dissolving the recovered products in anhydrous methanol.

1.4 Quantum chemistry calculations

Density functional theory (DFT) calculations were performed using the Gaussian 16 software package.[1] Geometry optimizations and frequency analyses were carried out at the B3LYP level of theory with the 6-311G(d) basis set.[2-4] Grimme's D3 dispersion correction with Becke–Johnson damping (GD3BJ) was employed to account for long-range dispersion interactions. To further analyze the nature of the interactions, wavefunction analysis was performed using the

Multiwfn program, and molecular visualizations were generated with Visual Molecular Dynamics (VMD).[5, 6]

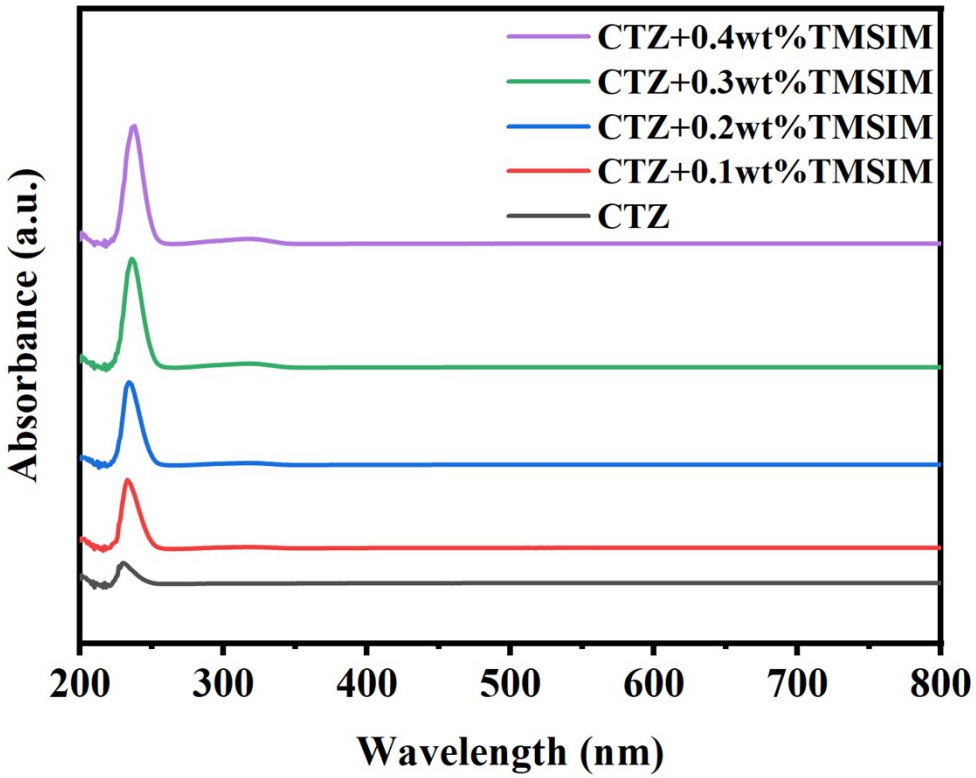

Figure S1. UV-vis absorption spectra of CTZ at a fixed concentration in acetonitrile with different TMSIM concentrations.

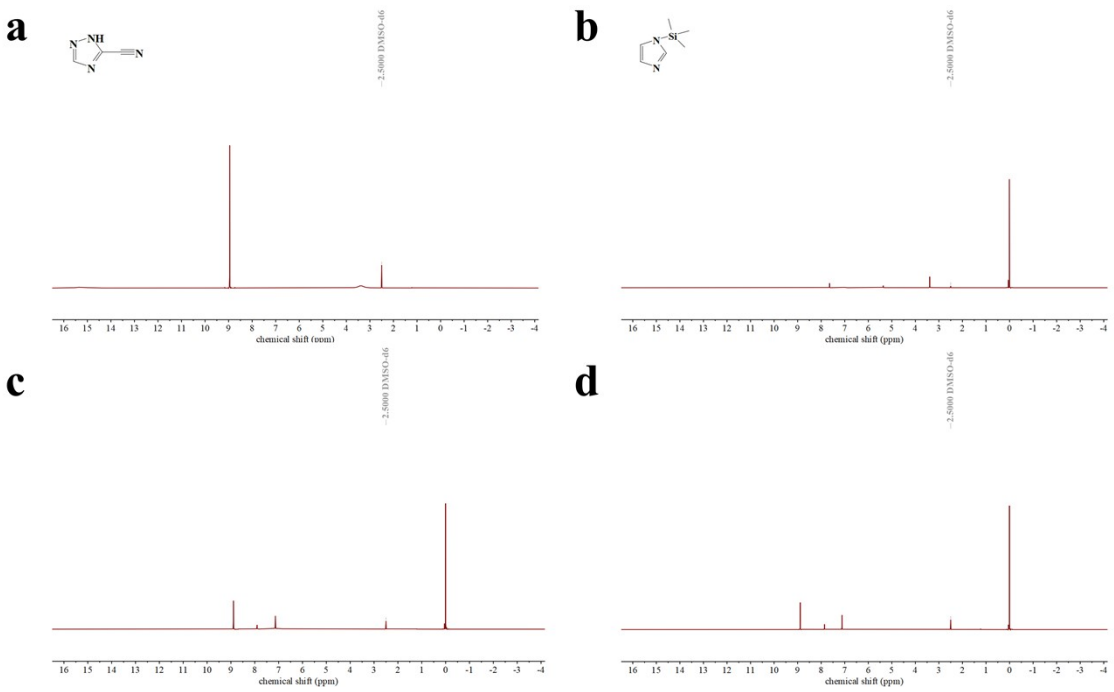

Figure S2. 1H NMR characterization of the CTZ-TMSIM interaction. Spectra of a) CTZ and b) TMSIM compared with CTZ:TMSIM mixtures at volume ratios of c) 4:1 and d) 3:2 (solvent: DMSO-d6).

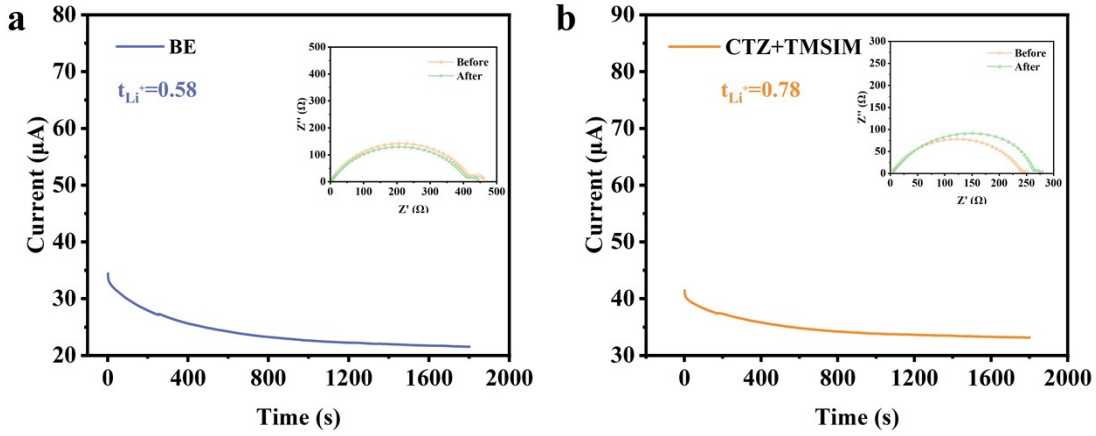

Figure S3. Li^+ transference number in different electrolyte systems (inset: EIS spectra of Li||Li symmetric cells before and after polarization)，a)BE，b)CTZ+TMSIM.

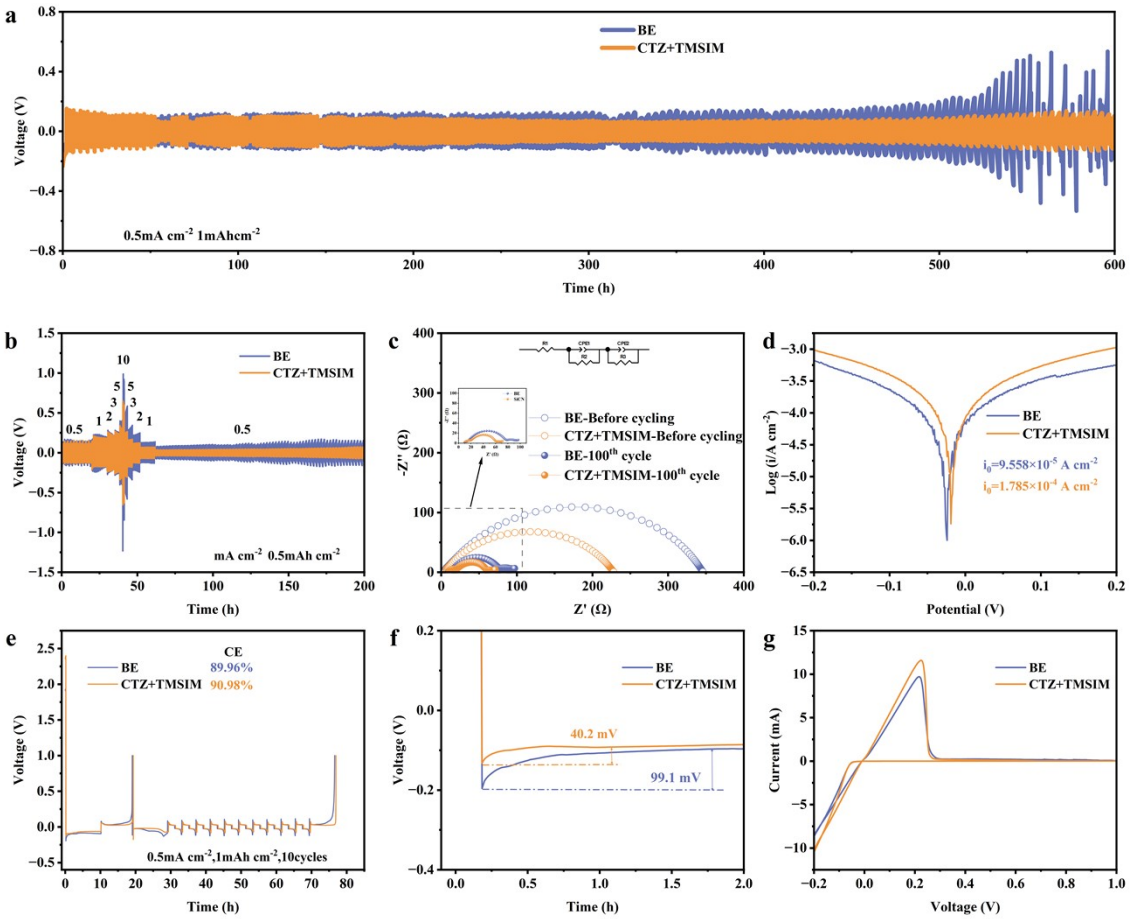

Figure S4. a) Cycling stability of Li||Li symmetric cells at 0.5 mA cm^{-2} with 1.0 mAh cm^{-2} capacity. b) Voltage–time profiles of Li||Li cells at various current densities. c) EIS spectra before cycling and after 100 cycles. d) Tafel plots of lithium plating/stripping under different electrolytes. e) Coulombic efficiency (CE) of Li||Cu half-cells at 0.5 mA cm^{-2} with 1.0 mAh cm^{-2} discharge capacity. f) Nucleation overpotentials during lithium plating in different electrolytes. g) CV curves of Li||Cu half-cells scanned at 0.5 mV s^{-1} from -0.2 V to 1 V.

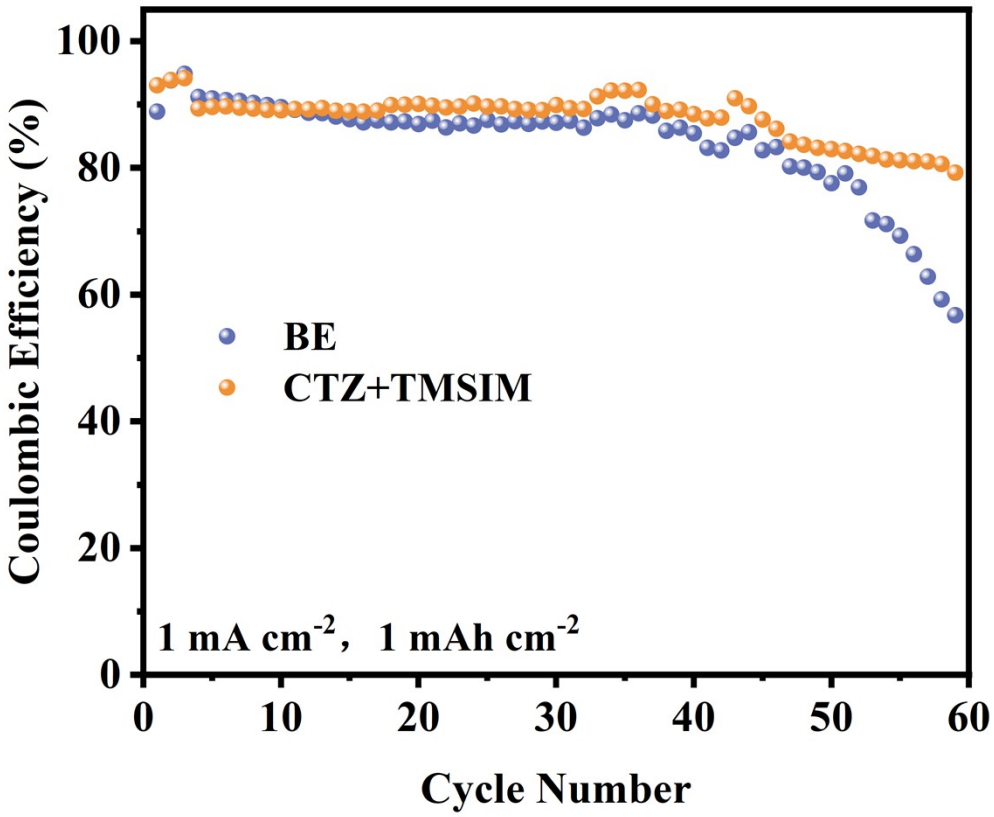

Figure S5. Comparison of Coulombic efficiencies of Li||Cu half-cells in different electrolytes.

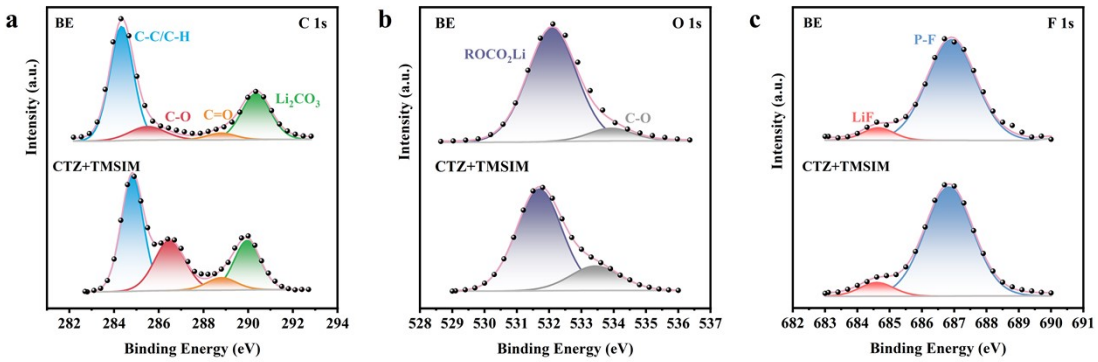

Figure S6. XPS spectra of the lithium metal anode in Li||Li symmetric cells after 50 cycles: a) C 1s, b) O 1s, c) F 1s.

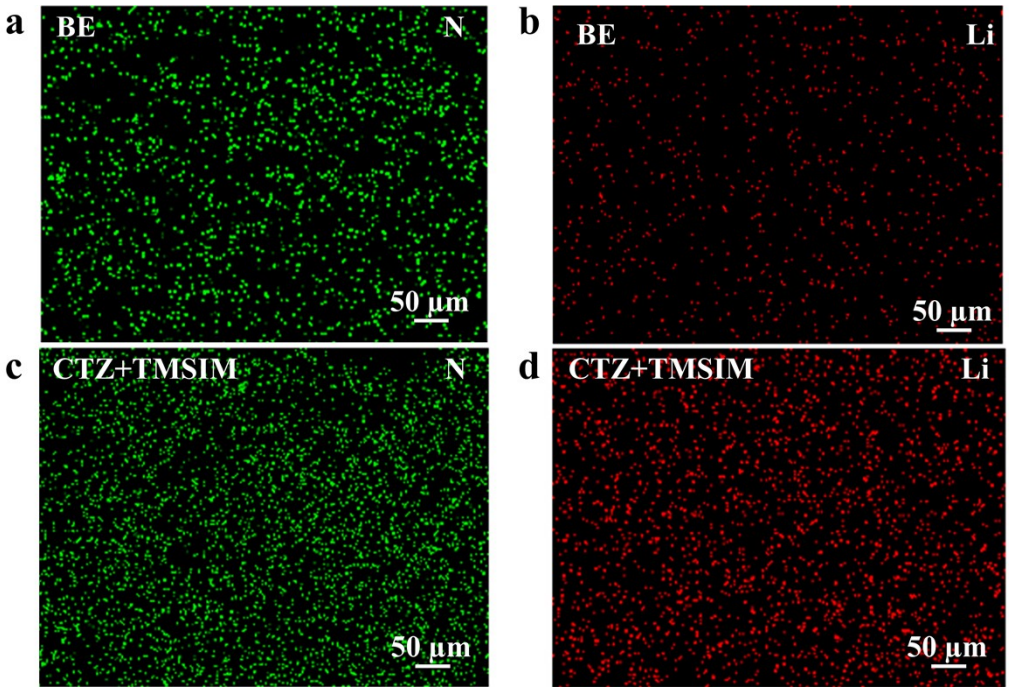

Figure S7. EDS mapping (scale bar: 50 μm) of the Li anode surface after 50 cycles for Li||Li symmetric cells.

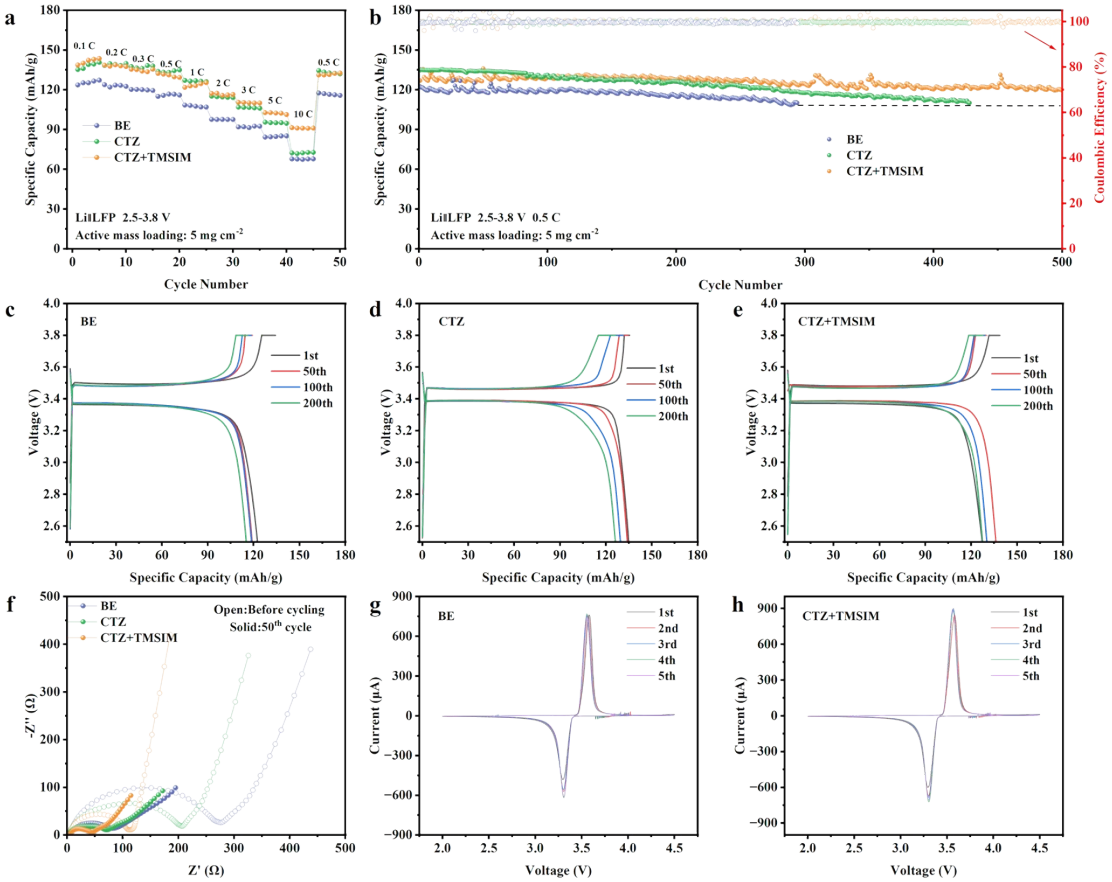

Figure S8. a) Rate performance of Li||LFP batteries; b) Long-term cycling performance of Li||LFP batteries at 0.5 C under different electrolytes; Charge-discharge curves of Li||LFP in c) BE, d) CTZ; e) CTZ+TMSIM electrolyte; f) Impedance comparison of Li||LFP batteries before cycling and after 50 cycles under different electrolyte systems. g) BE and h) CTZ+TMSIM electrolyte CV comparison for the first five cycles, voltage range 2-4.5 V, scan rate 0.1 mV s^{-1}.

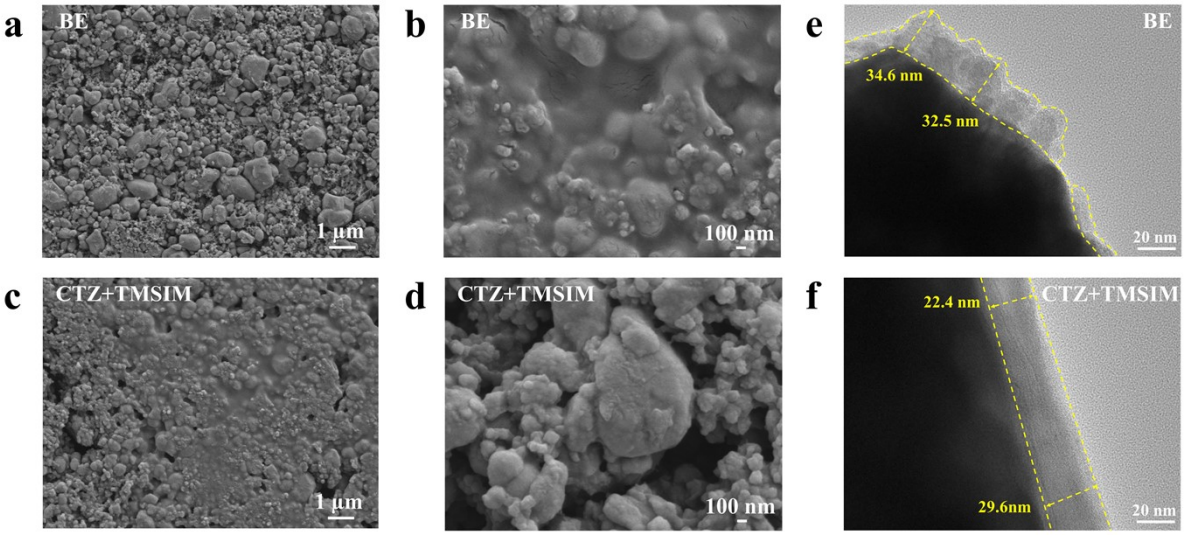

Figure S9. SEM images of LFP cathodes after 100 cycles: a, b) BE electrolyte; c, d) CTZ+TMSIM electrolyte. TEM images: e) BE electrolyte; f) CTZ+TMSIM electrolyte.

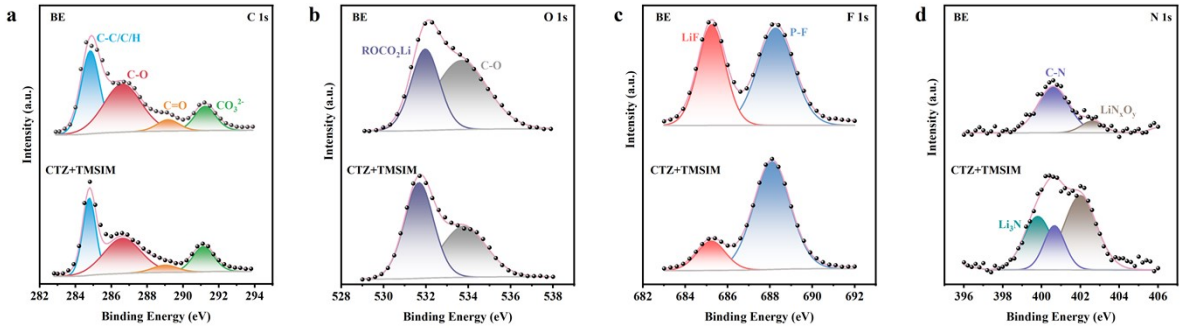

Figure S10. XPS spectra of LFP cathodes after 100 cycles in different electrolytes: a) C 1s, b) O 1s, c) F 1s, i) N 1s.

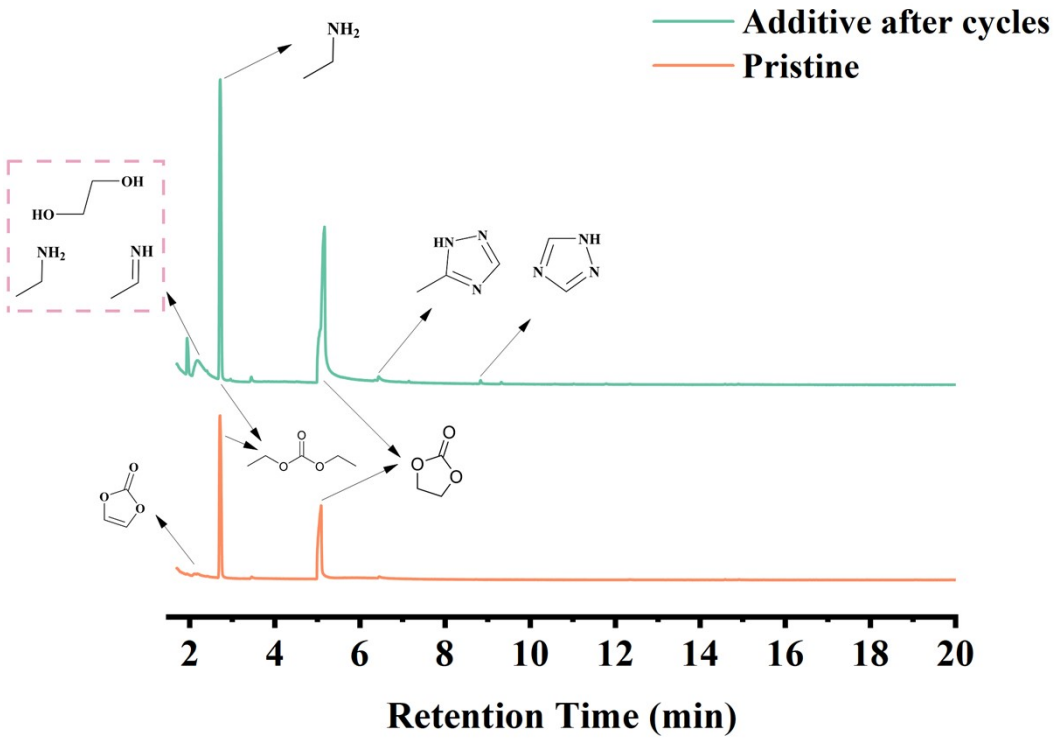

Figure S11. GC spectrum of the pristine electrolyte and CTZ+TMSIM electrolyte in Li||LFP cells after cycling.

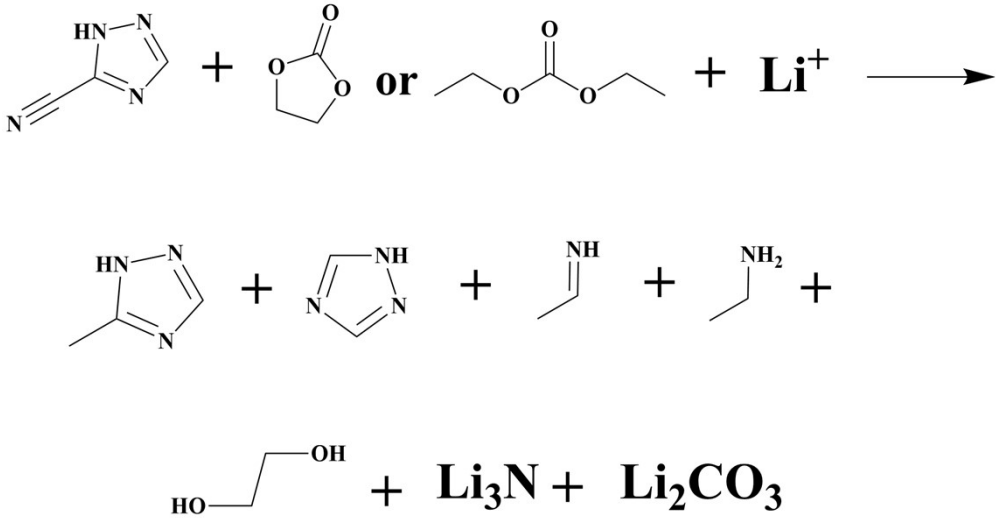

Figure S12. Proposed reaction equations potentially involving CTZ based on GC-MS results.

MS (MSD) (m/z, % rel. inten.): 62.04 ($[C_2H_6O]^+$, 25), 42.0 (100), 60.0 (28), 73.0 (100), 102.9 (20).**MS (MSD)** (m/z, % rel. inten.): 86.0 ($[C_3H_2O_3]^+$, 100), 42.0 (49), 57.9 (23). **MS (MSD)** (m/z, % rel. inten.): 88.02 ($[C_3H_4O_3]^+$, 64), 31.0 (27), 43.0 (100), 59.0 (18). **MS (MSD)** (m/z, % rel. inten.): 118.06 ($[C_5H_{10}O_3]^+$, 2), 31.0 (44), 45.0 (100), 63.0 (20), 91.0 (50). **MS (MSD)** (m/z): 43.04 ($[C_2H_5N]^+$, 100), 56.0 (1), 87.0 (1). **MS (MSD)** (m/z, % rel. inten.): 45.06 ($[C_2H_7N]^+$, 100), 31 (25), 59 (38), 77(50). **MS (MSD)** (m/z, % rel. inten.): 69.03 ($[C_2H_3N_3]^+$, 1), 43.0 (25), 110.0 (75), 127.0 (24), 140.0 (100). **MS (MSD)** (m/z, % rel. inten.): 83.05 ($[C_3H_5N_3]^+$, 36), 32.0 (26), 46.9 (24), 111.9 (100), 142.0 (100).

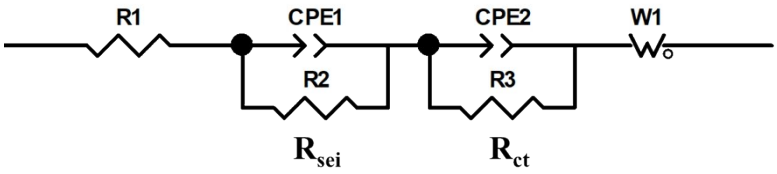

Table S1. EIS fitting results of Li||Li symmetric cells assembled with different electrolytes at various cycle numbers.

		BE	CTZ+TMSIM
Before cycling	R_{ct} **(Ω)**	190.35	117.65
	R_{sei} **(Ω)**	343.79	227.87
After 100th	R_{ct} **(Ω)**	45.39	37.56
	R_{sei} **(Ω)**	96.94	71.32

Table S2. Elemental analysis data of SEI formed in different electrolytes.

BE					CTZ+TMSIM				
Name	**Peak BE**	**FWHM eV**	**Area(P) CPS.eV**	**Atomic %**	**Name**	**Peak BE**	**FWHM eV**	**Area(P) CPS.eV**	**Atomic %**
C 1s	285.23	2.72	432435.03	44.05	C 1s	285.9	3.69	389906.12	40.19
O 1s	532.15	2.92	953024.78	40.16	O 1s	532.25	3.27	979277.75	41.74
F 1s	687.13	3.23	54705.52	1.84	F 1s	687.08	3.08	194026.25	6.61
P 2p	137.07	3.8	5326.83	0.37	P 2p	137.11	3.03	15115.33	1.05
N 1s	400.89	1	4834.07	0.32	N 1s	400.89	4.34	8348.16	0.55

Table S3. EIS fitting results of Li||LFP cells with different electrolytes at various cycle numbers.

		BE	CTZ	CTZ+TMSIM
Before cycling	$\mathbf{R_{ct}}$ **(Ω)**	150.96	112.53	59.38
	$\mathbf{R_{sei}}$ **(Ω)**	437.60	325.70	185.22
After 50th	$\mathbf{R_{ct}}$ **(Ω)**	46.28	40.02	23.59
	$\mathbf{R_{sei}}$ **(Ω)**	194.92	171.7	114.60

Notes and references

1. M. J. Frisch, G. W. Trucks, H. B. Schlegel, G. E. Scuseria, M. A. Robb, J. R. Cheeseman, G. Scalmani, V. Barone, G. A. Petersson, H. Nakatsuji, X. Li, M. Caricato, A. V. Marenich, J. Bloino, B. G. Janesko, R. Gomperts, B. Mennucci, H. P. Hratchian, J. V. Ortiz, A. F. Izmaylov, J. L. Sonnenberg, Williams, F. Ding, F. Lipparini, F. Egidi, J. Goings, B. Peng, A. Petrone, T. Henderson, D. Ranasinghe, V. G. Zakrzewski, J. Gao, N. Rega, G. Zheng, W. Liang, M. Hada, M. Ehara, K. Toyota, R. Fukuda, J. Hasegawa, M. Ishida, T. Nakajima, Y. Honda, O. Kitao, H. Nakai, T. Vreven, K. Throssell, J. A. Montgomery Jr., J. E. Peralta, F. Ogliaro, M. J. Bearpark, J. J. Heyd, E. N. Brothers, K. N. Kudin, V. N. Staroverov, T. A. Keith, R. Kobayashi, J. Normand, K. Raghavachari, A. P. Rendell, J. C. Burant, S. S. Iyengar, J. Tomasi, M. Cossi, J. M. Millam, M. Klene, C. Adamo, R. Cammi, J. W. Ochterski, R. L. Martin, K. Morokuma, O. Farkas, J. B. Foresman and D. J. Fox, *Gaussian 16 Revision A. 03*, Wallingford, CT, 2016.
2. M. P. Andersson， and P. Uvdal, *The Journal of Physical Chemistry A*, 2005, **109**, 2937–2941.
3. P. J. Stephens，, F. J. Devlin，, C. F. Chabalowski， and M. J. Frisch, *The Journal of Physical Chemistry A*, 1994, **98**, 11623–11627.
4. T. Yanai, D. P. Tew and N. C. Handy, *Chemical Physics Letters*, 2004, **393**, 51-57.
5. T. Lu and F. Chen, *Journal of Computational Chemistry*, 2011, **33**, 580-592.
6. William Humphrey, Andrew Dalke and a. K. Schulten, *Journal of Molecular Graphics*, 1996, **14**, 33-38.